

SCALINGS OF THE TEMPORALLY DEVELOPING TURBULENT PLANAR JET AND ITS TURBULENT/NON-TURBULENT INTERFACE

Sarp ER

Univ. Lille, CNRS, ONERA, Arts et Metiers
Institute of Technology, Centrale Lille Institut,
UMR 9014 - LMFL, F-59000 Lille, France
sarp.er.etu@univ-lille.fr

Jean-Philippe LAVAL

Univ. Lille, CNRS, ONERA, Arts et Metiers
Institute of Technology, Centrale Lille Institut,
UMR 9014 - LMFL, F-59000 Lille, France
jean-philippe.laval@univ-lille.fr

J. Christos VASSILICOS

Univ. Lille, CNRS, ONERA, Arts et Metiers Institute of Technology,
Centrale Lille Institut, UMR 9014 - LMFL, F-59000 Lille, France
john-christos.vassilicos@centralelille.fr

ABSTRACT

The temporally developing turbulent planar jet is examined starting from the fundamental conservation equations. We demonstrate that this flow is exceptional in that its mean flow scalings are the same for both equilibrium and non-equilibrium dissipation scalings. We also show that the average propagation velocity of the turbulent/non-turbulent interface (TNTI) is proportional to the global Reynolds number to a power which is inversely related to the fractal dimension of the iso-entropy surfaces which are all packed within the thin space composing the TNTI. Using a Direct Numerical Simulation (DNS) we confirm our theoretical predictions and show that the fractal dimension of these iso-entropy surfaces decreases from about 2.18 at the higher entropy values to between 2.1 and 2.05 at the lower ones. The average propagation velocity therefore increases from the higher to the lower entropy values, i.e. from the TNTI's inner, turbulent, edge to its purely viscous outer edge, in agreement with the constant mass flux through these inner layers.

INTRODUCTION

Turbulent shear flows are present in many natural and engineering processes. The TNTI delineating their turbulent extent is a central aspect of the entrainment mechanism whereby ambient potential fluid acquires vorticity when entrained into the turbulent flow. Investigation of the structure of this very thin interface and the local mechanisms driving the entrainment has been the subject of various studies (Corrsin & Kistler, 1955; Turner, 1986). The advent of DNS and Particle Image Velocimetry has brought a revival of studies of the TNTI over the past 20 years (Reeuwijk & Holzner, 2014; da Silva *et al.*, 2014; Mistry *et al.*, 2019).

Previous studies (Zhou & Vassilicos, 2017; Cafiero & Vassilicos, 2019) have shown that the scalings of the average TNTI propagation speed in spatially developing turbulent wakes and jets are different for different turbulence dissipation scalings. Two different types of turbulence dissipation scalings have been identified (Vassilicos, 2015), the non-equilibrium dissipation scalings and the classical Taylor-Kolmogorov dissipation scalings.

The aim of the present work is to establish the scalings of the average TNTI propagation speed in temporally developing planar turbulent jets and to see how they depend on turbulence dissipation. We start by obtaining a relation for the TNTI propagation velocity by considering the fractal nature of the interface and the generalized form of the dissipation scaling. We then present our DNS results on the mean flow and TNTI, and verify the relation obtained from our theoretical analysis against our DNS.

THEORETICAL ANALYSIS

In order to gain insight into the average propagation velocity v_n of the interface, we use the equality between the expansion rate of the turbulent jet volume and the flux through the TNTI,

$$\frac{dV_J}{dt} = Sv_n, \quad (1)$$

where S is the TNTI surface area and V_J is the volume of the turbulent jet. Following Zhou & Vassilicos (2017), we express dV_J/dt in terms of the jet half-width $\delta(t)$ and therefore write

$$\frac{d\delta}{dt} 2L_x L_z \sim Sv_n. \quad (2)$$

Here, L_x and L_z are the domain extents in x and z directions. Taking into account the fractal character of the interface (Sreenivasan *et al.*, 1989; Miller & Dimotakis, 1991; Flohr & Olivari, 1994; Mistry *et al.*, 2016), its surface area at spatial resolution r can be estimated as;

$$S(r) \sim L_x L_z \left(\frac{r}{\delta(t)} \right)^{(2-D_f)} \quad (3)$$

where D_f is the fractal dimension of the interface ($2 \leq D_f < 3$). To estimate the actual surface area of the interface we need

to estimate the smallest relevant length-scale r_{min} . Considering that a surface with a finite thickness cannot fold with a radius smaller than its thickness, the interface thickness can be used as the minimal length scale. We assume that this length scale is proportional to the Corrsin length-scale $\eta_I \sim \nu/v_n$ (Corrsin & Kistler, 1955), where ν is the kinematic viscosity of the fluid. We therefore arrive at

$$\frac{d\delta}{dt} \sim \left(\frac{\nu}{v_n \delta} \right)^{(2-D_f)} v_n \quad (4)$$

from eq. 2. We now need to obtain the time-evolution of the jet half-width $\delta(t)$, in order to proceed with eq. 4 and obtain an expression for v_n .

We conduct the analysis of the temporally developing turbulent jet flow starting from the conservation of mass and momentum by assuming self-similarity of turbulent profiles in the form $\phi = \phi_0(t)f(y/\ell(t))$ for a variable ϕ , where $\phi_0(t)$ is the amplitude and $\ell(t)$ is the time varying length scale. The volume flux is conserved for the temporally developing planar jet case, i.e. $\frac{\partial}{\partial t} \int_{-\infty}^{\infty} \langle u \rangle dy = 0$, unlike spatially developing jets. It was shown that mean flow scalings differ for different dissipation scaling regimes by Cafiero & Vassilicos (2019) for spatially developing planar jets. In order to investigate if there is a similar behavior in temporally developing planar jets, we pursue our analysis by using the turbulent kinetic energy equation and the general dissipation scaling $\varepsilon_0 \sim \left(\frac{Re_G}{Re_0} \right)^m \frac{K_0^{3/2}}{\delta}$, where Re_G is a global Reynolds number, determined by the initial jet velocity and jet width ($Re_G = U_J H_J / \nu$) and $Re_0(t) = K_0(t) \delta(t) / \nu$ is a local Reynolds number which varies in time. The classical equilibrium dissipation scaling is retained for $m = 0$, and $m \neq 0$ leads to non-equilibrium dissipation scalings. The following mean flow scalings are found as a result;

$$u_0 \sim (U_J H_J)^{1/2} (t - t_0)^{-1/2}, \quad (5)$$

$$\delta \sim (U_J H_J)^{1/2} (t - t_0)^{1/2}, \quad (6)$$

where u_0 is the center-plane mean flow velocity and t_0 is a virtual origin. A peculiar feature of this problem is that the mean flow scalings are independent of the exponent m in the dissipation relation, thus insensitive to the different dissipation regimes. The fact that the mean flow scalings are the same for both equilibrium and non-equilibrium dissipation scalings is exceptional as this is not the case in turbulent axisymmetric wakes and spatially developing turbulent planar jets, where different scalings for u_0 and δ are shown to hold for different dissipation regimes in Dairay *et al.* (2015); Cafiero & Vassilicos (2019).

From eq. 4 and eq. 6 one can obtain the following relation for v_n :

$$v_n \sim (U_J H_J)^{1/2} (t - t_0)^{-1/2} Re_G^{(2-D_f)/(D_f-1)}. \quad (7)$$

Eq. 7 shows that the average TNTI propagation velocity is proportional to the global Reynolds number to the power $\frac{2-D_f}{D_f-1} = \frac{1}{D_f-1} - 1$ which is inversely related to D_f .

The scalings of the inner turbulent length scales can also be obtained. By using the relation; $\eta = (\nu^3/\varepsilon_0)^{1/4}$ and the dissipation scaling relation, the Kolmogorov length scale η can be written as;

$$\eta \sim (U_J H_J)^{1/2} (t - t_0)^{1/2} Re_G^{-3/4}. \quad (8)$$

As for the Taylor length scale λ , the relation $\varepsilon_0 \sim \nu K_0 / \lambda^2$ is employed with the Townsend's relation $K_0 \sim R_0$ (Townsend, 1976);

$$\lambda \sim (U_J H_J)^{1/2} (t - t_0)^{1/2} Re_G^{-1/2} \quad (9)$$

The velocities related to these length scales can be written as $u_\eta \sim (U_J H_J)^{1/2} (t - t_0)^{-1/2} Re_G^{-1/4}$ and $u_\lambda \sim (U_J H_J)^{1/2} (t - t_0)^{-1/2} Re_G^{-1/2}$. Comparing these inner velocity scalings with eq. 7, it can be seen that v_n has similar Re_G -dependence with u_η and u_λ for different values of D_f , i.e. $v_n \sim u_\eta$ when $D_f = 7/3$ and $v_n \sim u_\lambda$ when $D_f = 3$.

SIMULATION DETAILS

A set of simulations of temporally developing planar jets have been carried out with a pseudo-spectral solver with periodic boundary conditions in all three directions. The simulations were run in a domain of size $(8H_J, 12H_J, 8H_J)$ with resolution $1024 \times 1536 \times 1024$ in directions x, y and z respectively, such that the spatial resolution is the same in all the three directions and is smaller than the Kolmogorov length scale calculated on the center-plane throughout the time evolution of the jet as shown in the figure 1, where $T_{ref} = H_J / (2U_J)$ is used for the non-dimensionalization of time. The time integration was carried out with a second order Runge-Kutta time stepping scheme. Apart from the $2/3$ truncation for de-aliasing, a filtering function which is only effective at the highest resolved wavenumbers was also applied to obtain smooth enstrophy isosurfaces at the outer edge of the TNTI. This additional filtering was found to be very effective for eliminating numerical oscillations at near-zero enstrophy levels. The initial velocity profile of the jet is (Reeuwijk & Holzner, 2014; da Silva & Pereira, 2008);

$$U(y) = \frac{U_J}{2} - \frac{U_J}{2} \tanh \left[\frac{H_J}{4\theta_0} \left(1 - \frac{2|y|}{H_J} \right) \right], \quad (10)$$

where $y = 0$ is the center-plane of the planar jet and θ_0 is the initial momentum thickness. $H_J / \theta_0 = 35$ is chosen similarly to other studies, as this value leads to a faster transition compared to lower H_J / θ_0 values when perturbed by high amplitude noise (da Silva and Pereira, 2008). A white-noise is added on top of the mean velocity profile and the noise is filtered by the velocity profile, thus the region outside the turbulent jet is free from random oscillations. The amount of enstrophy added with the white noise corresponds to 4% of the enstrophy peaks of the mean profile.

RESULTS

Scaling of the Mean Flow

The analysis of the DNS data starts with the investigation of the mean flow characteristics of the planar jet, in order to determine when the jet becomes fully turbulent and the self-similar regime is established.

The self-similar regime is the range, where the dynamics of the problem evolve with a local amplitude scaling and a local length scale, i.e. $\phi_0(t)$ and $\ell(t)$, so that the time dependent mean profile of a variable ϕ can be written in the form $\phi = \phi_0(t)f(y/\ell(t))$ (Townsend, 1976). For the investigation of the self-similarity of the mean flow profiles, we start by normalizing the profiles by using the local length scale, jet half-width $\delta(t)$, in figure 2a.

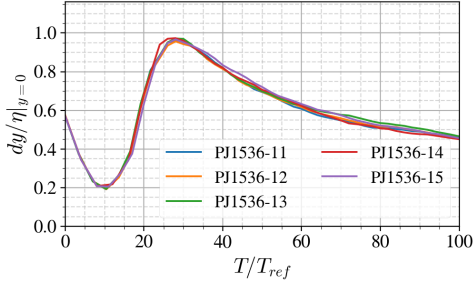


Figure 1: Spatial resolution dy/η of the simulations plotted versus normalized time.

The expansion of the jet can be seen in figure 2b, where $\delta^2/H_j^2 \sim t$ behavior is compatible with eq.6. Here the jet half-width $\delta(t)$ is defined by the condition that the mean streamwise velocity at a given y location is half of the mean streamwise velocity at the center-plane, $\bar{U}(y = \delta, t) = U_c(t)/2$, where $U_c(t) = \bar{U}(y = 0, t)$. An important feature of the temporally

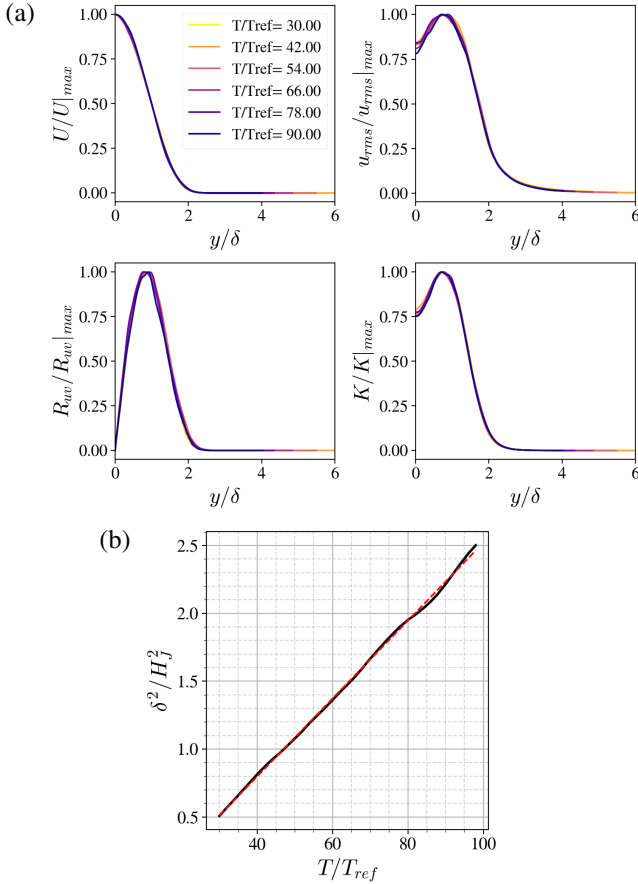


Figure 2: (a) Self-similar, normalized profiles of mean flow U , stream-wise turbulence intensity u_{rms} , Reynolds shear stress R_{uv} and turbulent kinetic energy K . (b) Jet half-width squared, δ^2/H_j^2 , versus time.

developing planar jet is that Re_λ remains constant due to the inverse relationship between the scalings of u_0 and λ , which also suggests that all length scales evolve identically as time progresses. Constancy of Re_λ can be seen in figure 3a and the time evolution of the ratios λ/η and δ/λ is given in the figure

3b. The outer length scale of the problem, δ , has also the same time dependency as λ and η .

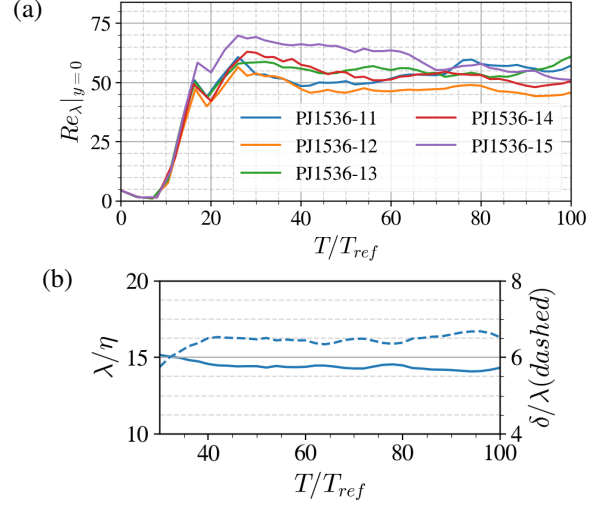


Figure 3: (a) Time evolution of Re_λ calculated at the centre-plane ($y = 0$). (b) Ratios of length scales λ/η and δ/λ throughout time.

Looking at the mean flow scalings, it is also observed that the $\frac{u_0 \delta}{U_j H_j / 2} \sim 1$ for all the investigated time range, attesting to the constant volume flux throughout the time evolution of the flow. Townsend's relation, $K_0 \sim R_0$ holds until $T/T_{ref} = 80$, and after that the ratio K_0/R_0 starts to decrease. This is a probable demarcation of boundary effects on the jet as it expands significantly compared to the domain extent in y -direction.

Identification of the TNTI

The TNTI is a very sharp interface between the turbulent and non-turbulent regions of the flow. Thus, a quantity related to the turbulent flow should be used to distinguish the two flow regimes. In this study we use the enstrophy as the TNTI detection criterion, $\omega^2(x, y, z) = \omega_{th}^2$, similar to other studies in the literature (Reeuwijk & Holzner, 2014; Zhou & Vassilicos, 2017). Unlike some other studies, various threshold values are used to locate the different iso-surfaces constituting the TNTI. In order to see the enstrophy values marking the TNTI, the volume where $\omega^2(x, y, z) > \omega_{th}^2$ is plotted for a wide range of threshold values in figure 4. The plateau over a wide range of $\omega^2(x, y, z)_{th} / \omega^2(x, y, z)_{ref}$ marks the TNTI region. This plateau forms due to the fact that the enstrophy iso-surfaces are positioned very close to each other spatially. By picking a threshold value, which falls inside the plateau, one can detect the iso-surface which envelopes the turbulent jet but also the irrotational fluid pockets which are completely engulfed into the turbulent region. In this study, we detect these pockets, and the iso-surfaces related to these pockets are not taken into account. Thus, we are only left with the continuous iso-surface that envelopes the jet from outside.

Fractal Dimension of the TNTI

An important term in the relation 7 for the mean TNTI propagation velocity v_n involves the fractal dimension of the surface D_f . D_f is present in the term responsible for the Re dependence of v_n . After the detection of the 3D TNTI surface,

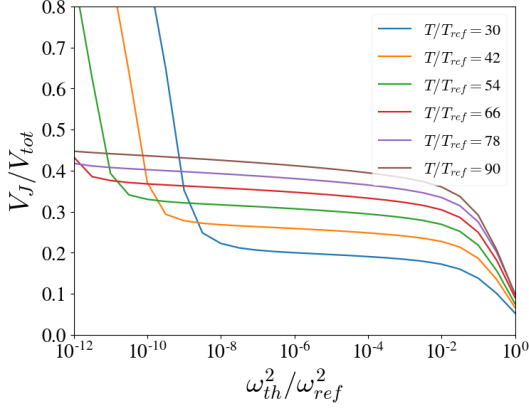


Figure 4: The volume which satisfies the condition of $\omega^2(x, y, z) > \omega_{th}^2$ is plotted for a wide range of thresholds ω_{th}^2 .

a box-counting algorithm is utilized for the calculation of its fractal dimension. Briefly stated, the surface S is covered with cubes with varying edge sizes r (Mandelbrot, 1982). By looking at the $\log - \log$ variation of the number N of boxes needed to cover the surface, with varying box-size r , the fractal dimension D_f is calculated for a chosen threshold value ω_{th}^2 at a given instant. The independent parameters which D_f may de-

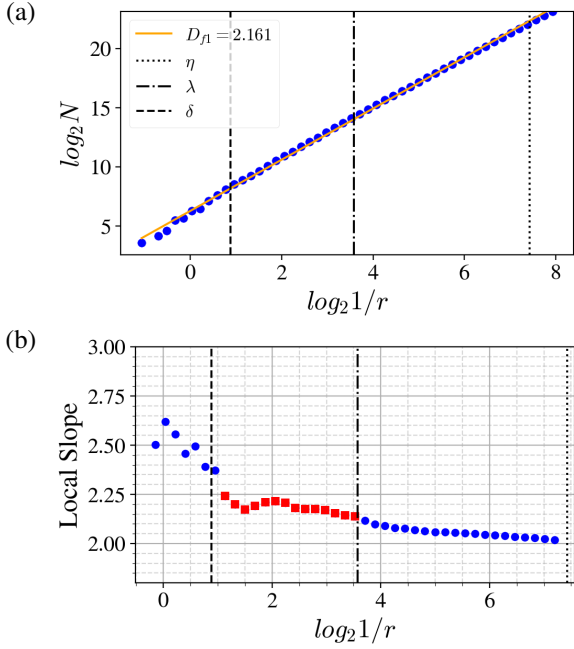


Figure 5: (a) The number N of boxes needed to cover the TNTI surface, versus inverse box-size $1/r$ plotted in a $\log - \log$ scale and (b) the local slope of the $\log_2 N - \log_2(1/r)$.

pend on are the measurement length scale r , time T/T_{ref} and the enstrophy threshold $\omega_{th}^2/\omega_{ref}^2$. The dependence on r is the first to investigate. Even though the TNTI surface shows fractal characteristics, it is also known that for very small scales, diffusive processes smooth out the contortions. Thus the slope of the $\log_2 N - \log_2(1/r)$ plot is expected to reduce to $D_f = 2$. Looking at figure 5a, the orange line is the slope with all the

data points included. But it is found that this way of calculation of D_f , shown as D_{f1} in the figure legend, leads to inaccurate values due to the variation of the slope with r . In order to find the linear region of the $\log_2 N - \log_2 1/r$ plot, local slopes of the data points are calculated by fitting nine points at a time. Linear fits are made for each set, and their slope is plotted as the local slope at that location in figure 5b. Considering a wide range of thresholds and the time range after the transition to turbulence of the jet, it is observed that a plateau of the local slope is present between the scales δ and λ (as can be observed for example from figure 5b). For the scales $r < \lambda$ the local slope reduces towards the value of 2. Thus the average of local slope values in this region (marked in red in figure 5b) is used for the calculation of D_f , denoted as D_{f2} , with the exception of the first point from the side of δ as it introduces oscillations because N is not well converged for large box sizes. Figure 6a shows D_{f2} values calculated for various

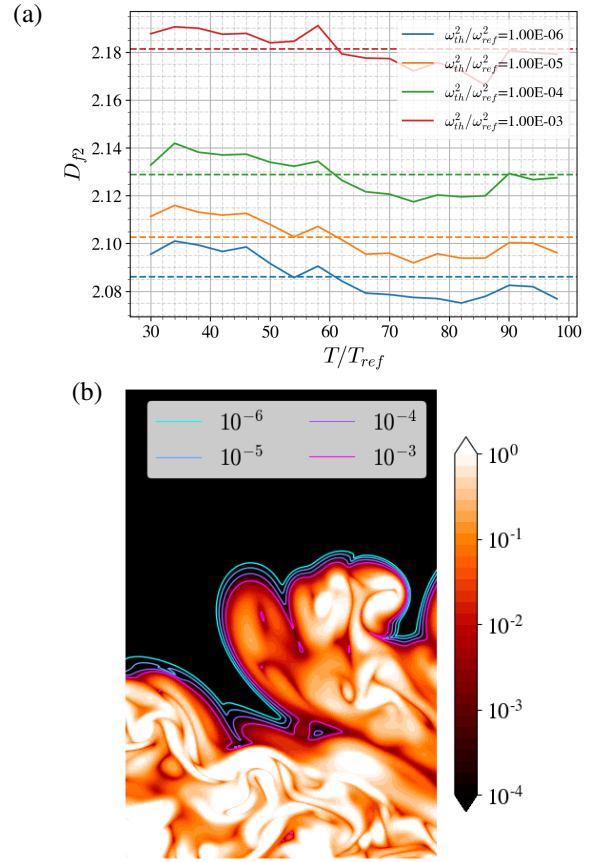


Figure 6: (a) Variation of the fractal dimension throughout the TNTI with different $\omega_{th}^2/\omega_{ref}^2$ values and their constancy in time. (b) a section of the TNTI, where different iso-surfaces of ω_{th}^2 are shown on top of $\log_{10}(\omega_{th}^2/\omega_{ref}^2)$ contours. Iso-contours from cyan to pink are $\omega_{th}^2/\omega_{ref}^2 = 10^{-6}, 10^{-5}, 10^{-4}$ and 10^{-3} .

enstrophy thresholds for a range of times. It is observed that the D_f values remain approximately constant in time with a very slight variation. D_f is seen to vary significantly with enstrophy thresholds. It tends to have a higher value on the turbulent side of the TNTI, i.e. $D_f \approx 2.18$ for $\omega_{th}^2/\omega_{ref}^2 = 10^{-3}$ and reduces to $D_f \approx 2.085$ for $\omega_{th}^2/\omega_{ref}^2 = 10^{-6}$. This trend can be seen qualitatively from figure 6b, where the iso-surfaces of

higher enstrophy values towards the inner side of the TNTI are more contorted compared to the iso-surfaces at the outer edge.

Average Propagation Velocity of the TNTI

The average propagation velocity of the TNTI into the non-turbulent region is obtained by using eq.7. The time derivative of the jet half-width $d\delta/dt$ is obtained from the mean flow profiles and the surface area S is measured by the box-counting algorithm. The v_n profiles calculated over enstrophy thresholds are shown in figure 7a. The propagation velocity is observed to be higher in the non-turbulent side where $\omega_{th}^2/\omega_{ref}^2$ takes smaller values and it is reduced towards the higher thresholds. This is compatible with the constancy of the flux throughout the TNTI, $Q = Sv_n$, and thus the relation between the surface area and propagation velocity becomes $S \sim 1/v_n$. As the inner iso-surfaces are more contorted, their surface area S is higher than the outer iso-surfaces. Figure 7b shows the TNTI propagation velocity v_n normal-

turbulent region, other mechanisms begin to be as active as the viscous diffusion, thus causing the deviation observed in the figure 7b.

CONCLUSIONS AND DISCUSSION

The temporally developing planar jet has been analyzed starting from the basic conservation equations. The evolution of the time-developing turbulent planar jet is fundamentally different from the evolution of its space-developing counterpart. It is the volume flux which is being conserved throughout the time evolution of the temporal jet. More importantly, Re_λ remains constant after the jet becomes fully turbulent. This implies that the inner turbulent length scales evolve together in time. In addition, the mean flow length scale, i.e. the jet half-width, varies in a similar manner, thus all the length scales of the problem have identical $t^{1/2}$ power law evolutions in time. The corresponding velocity scales also decay identically with each other as $t^{-1/2}$. As shown in (Cafiero & Vassilicos, 2019), the non-equilibrium dissipation scaling leads to different scalings of the mean flow than the equilibrium dissipation scaling for spatially developing planar jets. Similar analysis has been conducted to discover the implications of the non-equilibrium dissipation scaling on the evolution of the temporally developing jet, but it has been found that the time evolution of the mean flow parameters are insensitive to the turbulence dissipation scalings. By considering the fractal nature of the TNTI and the self-similarity of the turbulent jet, a relation is obtained for the average propagation velocity of the interface v_n . This relation shows that v_n is proportional to the global Reynolds number raised to a power which is inversely related to the fractal dimension of the surface. Our DNS supports this relation and the assumptions and predictions of our theory and reveals an interesting inner structure of the TNTI with a dependence of the fractal dimension on iso-enstrophy levels. It is shown that the fractal dimension D_f of the enstrophy iso-surfaces vary throughout the thickness of the TNTI. D_f values are smaller at the outer edge of the TNTI, and increase towards the turbulent region. Thus the outer edge of the TNTI is less contorted compared to the turbulent side where the surface is more irregular and the surface is higher. The TNTI propagation velocity is found to be higher at the outer edge and lower on the turbulent side, which agrees with the constancy of the entrainment flux throughout the thickness of the TNTI, $Q = Sv_n$. The v_n normalized by the term responsible for the D_f dependence remains approximately constant for the range of thresholds falling into the TNTI, supporting the relation found for v_n .

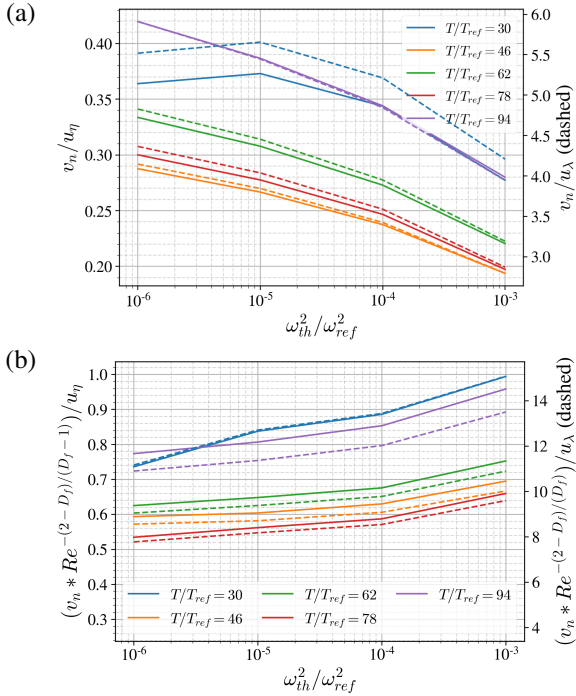


Figure 7: (a) Average interface propagation velocity, v_n , normalized by u_η (solid lines, left axis) and by u_λ (dashed lines, right axis) for different threshold values. (b) v_n pre-multiplied by the $Re^{f(D_f)}$ with same normalizations.

ized by the term responsible for the dependence on D_f , i.e. $Re_G^{(2-D_f)/(D_f-1)}$ in the eq. 7. $v_n/Re_G^{(2-D_f)/(D_f-1)}$ remains approximately constant for the thresholds which fall into the enstrophy range of TNTI, which confirms the D_f dependence found with the theoretical analysis. It is observed that the constancy of the normalized v_n starts to deviate at the higher enstrophy values. To better understand this, it must be remembered that the Corrsin length $\eta_l \sim v/v_n$ is used as the smallest length scale on the TNTI for obtaining eq. 7. This length scale is obtained by assuming that it is the viscous diffusion mechanism that drives the process of irrotational fluid packets obtaining vorticity at the TNTI. As we go further inside the

ACKNOWLEDGEMENTS

This work is supported by JCV's Chair of Excellence Co-PreFlo funded by I-SITE-ULNE (grant number R-TALENT-19-001-VASSILICOS); MEL (grant number CONVENTION-219-ESR-06) and Region Hauts de France (grant number 20003862). This work was granted access to the HPC resources of IDRIS under the allocation 021741 made by GENCI (Grand Equipment National de Calcul Intensif).

REFERENCES

- Cafiero, G. & Vassilicos, J. C. 2019 Non-equilibrium turbulence scalings and self-similarity in turbulent planar jets. *Proceedings of the Royal Society A* **475** (2225), 20190038.
Corrsin, S. & Kistler, A.L. 1955 Free-stream boundaries of turbulent flows. *Tech. Rep.* January. NACA.

- Dairay, T., Obligado, M. & Vassilicos, J. C. 2015 Non-equilibrium scaling laws in axisymmetric turbulent wakes. *Journal of Fluid Mechanics* **781**, 166–195.
- Flohr, P. & Olivari, D. 1994 Fractal and multifractal characteristics of a scalar dispersed in a turbulent jet. *Physica D: Nonlinear Phenomena* **76** (1-3), 278–290.
- Mandelbrot, Benoit B. 1982 *The fractal geometry of the nature*. New York: W. H. Freeman & Co.
- Miller, Paul L. & Dimotakis, Paul E. 1991 Stochastic geometric properties of scalar interfaces in turbulent jets. *Physics of Fluids A* **3** (1), 168–177.
- Mistry, D., Philip, J. & Dawson, J. R. 2019 Kinematics of local entrainment and detrainment in a turbulent jet. *Journal of Fluid Mechanics* **871**, 896–924.
- Mistry, D., Philip, J., Dawson, J. R. & Marusic, I. 2016 Entrainment at multi-scales across the turbulent/non-turbulent interface in an axisymmetric jet. *Journal of Fluid Mechanics* **802**, 690–725.
- Reeuwijk, M. V. & Holzner, M. 2014 The turbulence boundary of a temporal jet. *J. Fluid Mech.* **739**, 254–275.
- da Silva, Carlos B., Hunt, J. C. R., Eames, Ian & Westerweel, Jerry 2014 Interfacial layers between regions of different turbulence intensity. *Annual Review of Fluid Mechanics* **46** (1), 567–590.
- da Silva, Carlos B. & Pereira, José C. 2008 Invariants of the velocity-gradient, rate-of-strain, and rate-of-rotation tensors across the turbulent/nonturbulent interface in jets. *Phys. Fluids* **20** (055101), 1–18.
- Sreenivasan, K. R., Ramshankar, R. & Meneveau, C. 1989 Mixing, entrainment and fractal dimensions of surfaces in turbulent flows. *Proceedings of the Royal Society A: Mathematical, Physical and Engineering Sciences* **421** (1860), 79–108.
- Townsend, A. A. 1976 *The structure of turbulent shear flow*, 2nd edn. Cambridge University Press.
- Turner, J. S. 1986 Turbulent entrainment: the development of the entrainment assumption, and its application to geophysical flows. *Journal of Fluid Mechanics* **173**, 431–471.
- Vassilicos, J. C. 2015 Dissipation in turbulent flows. *Annual Review of Fluid Mechanics* **47** (1), 95–114.
- Zhou, Y. & Vassilicos, J. C. 2017 Related self-similar statistics of the turbulent/non-turbulent interface and the turbulence dissipation. *Journal of Fluid Mechanics* **821**, 440–457.